# Appendix

## A1. Overtopping model

Figure A1.1 indicates a typical bathymetric profile for Hulhumalé. The focus on this study has been on the eastern side of the island where the overtopping modelling took place as this part of the island is most exposed to the open ocean and long period waves which may induce flooding. The text in red in Figure A1.1 indicates the different future conditions tested according to the magnitude of sea-level rise and adaptation conditions (see A2).

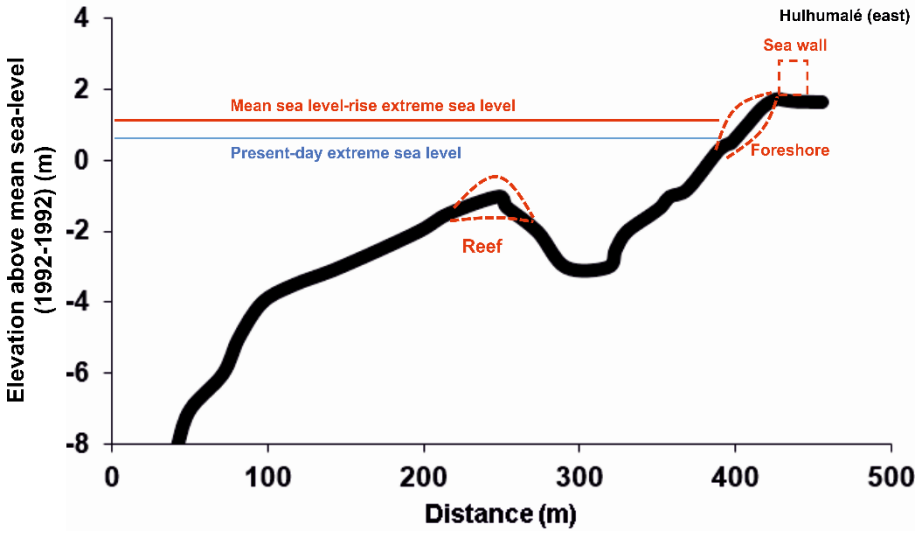


Figure A1.1 Typical bathymetry on the eastern shore of Hulhumale.

Significant wave height, period, duration of design storm, still water and extreme water level conditions (as described in Wadey et al. 2017) were extracted from data sources as described in Section 2.2. These were input, along with bathymetry data into a semi-implicit Shallow-water and Boussinesq (SWAB) numerical model (McCabe, 2011; McCabe et al., 2013; Stansby et al., 2013). A typical profile of the SWAB model is shown in Figure A1.2.

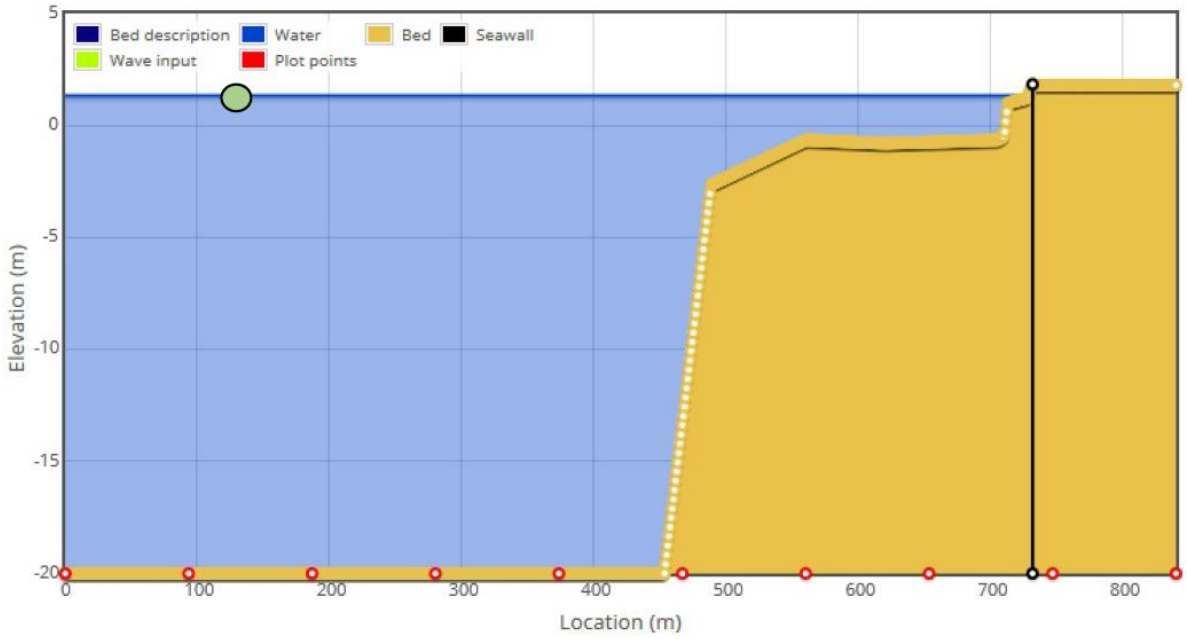


Figure A1.2. Example of the profile and user interface of the SWAB model. The bed along the x-axis is flattened at 450m for modelling purposes only. The elevation on the y-axis represents the datum above mean sea-level (1992-1993). The black vertical line represents the location of the sea wall.

SWAB uses a Boussinesq modelling approach allowing for the breaking of a wave and its propagation over the surf zone, and the lagoon area where the water is deeper than the immediate reef edge. It simulates nearshore waves, run-up and overtopping. SWAB has previously been used and tested against field data and wave flume tests for sites in the UK (McCabe et al. 2013). Overtopping comparisons have been in the 'bounds of accuracy' of what might be expected, given the inherit uncertainty of datasets used.

To determine the volume of overtopping per metre run, SWAB solves the continuity equation (Equation A1.1) and momentum equation (Equation A1.2) of Madsen and Sorensen (1992):

$$\frac{\partial h}{\partial t} + \frac{\partial (\mathrm{hu})}{\partial x} = 0. \qquad \text{Equation A1.1}$$

$$\frac{\partial (\mathrm{hu})}{\partial t} + \frac{\partial (\mathrm{hu}^2)}{\partial x} = -\mathrm{gh}\frac{\partial h}{\partial x} - \mathrm{gh}\frac{\partial z_b}{\partial x} - \frac{\tau_b}{\rho} + \left\{\left(B + \frac{1}{3}\right) d^2 \left(\frac{\partial^3 (\mathrm{hu})}{\partial x^2 \partial t}\right) + \mathrm{Bgd}^3 \frac{\partial^3 \eta}{\partial x^3} + d\frac{\partial d}{\partial x}\left(\frac{1}{3}\frac{\partial^2 (\mathrm{hu})}{\partial x \partial t} + 2\mathrm{Bgd}\frac{\partial^2 \eta}{\partial x^2}\right)\right\}_{\mathrm{pre-break}} + \left\{\frac{\partial}{\partial x}\left(h(\nu + \nu_e)\frac{\partial u}{\partial x}\right)\right\}_{\mathrm{post-break}}$$

Equation A1.2

Where:

$B$ = constant that controls the linear dispersion characteristics;

$d$ = still-water depth (m);

$g$ = gravitation acceleration (m/s);

$h$ = water depth (m);

$t$ = time (s);

$u$ = horizontal depth-averaged velocity, in the x-direction (m $s^{-1}$);

$\nu$ = kinematic viscosity of water ($m^2s^{-1}$);

$\nu_e$ = wave breaking eddy viscosity ($m^2s^{-1}$);

$x$ = location in profile or grid domain (m);

$z_b$ = bed level above datum level (m);

$\eta$ = Free surface level above datum level (m)

$\rho$ = water density (kg $m^{-3}$);

$\tau_b$ = bed shear stress (N $m^{-2}$);

The Boussinesq terms are the pre-breaking part on the second line of Equation A1.2. Madsen and Sorensen (1992) determined that a value of $B$ = 1/15 gives the best linear dispersion characteristics. The breaking of waves is expected to occur when the wave height to water depth ratio exceeds 0.6 (McCabe 2011; McCabe et al. 2013). In the surf zone, the pre-breaking Boussinesq terms are set to zero giving the nonlinear shallow-water equations. A post-breaking horizontal diffusion term is also applied (the third line of Equation A1.2), similar to the method in Kennedy et al. (2000).

The nonlinear shallow water equations do not take account of the impact force imposed by a sea wall when a jet (or wave) of water impacts against a wall in the $x$ direction. If a jet of water with velocity $u_{jet}$ is reflected backwards at the same speed (possible with a recurve wall) then the force imposed by the wall on the water, $F_{wall}$:

$$F_{\mathrm{wall}} = 2\rho \mathrm{A} \mathrm{u}_{\mathrm{jet}^2}$$

Equation A1.3

Where:

$A$ = Cross-sectional area of the jet of water ($m^2$)

$F_{wall}$ = Force imposed by the wall on the water (N);

$u_{jet}$ = Water velocity in the horizontal direction (m $s^{-1}$);

$\rho$ = water density (kg $m^{-3}$);

In reality, when a wave impacts against a seawall, the flow is directed upwards as well as seawards and the following term is applied to the momentum equation (A1.2), at cell *i*, located at the wall:

$$F_{\mathrm{wall},i} = \frac{k_{\mathrm{wall}} h_{F,i} u_i^2}{\Delta x}$$

Equation A1.4

Where:

$F_{wall,I}$ = force per water density per unit bed area, imposed on the flow ($m^2 s^{-2}$)

i = cell, as represented in the model;

$k_{\mathrm{wall}}$ = empirical constant;

$h_{F,i}$ = water depth in front of the wall (but less than the height of the wall itself) (m);

$u_i$ = horizontal water velocity impacting the wall (m $s^{-1}$);

$\Delta x$= cell size (m).

The value of $k_{\mathrm{wall}}$ is likely to be a function of the profile of the wall, although $k_{\mathrm{wall}}$ = 0 when the flow is directed seawards (i.e. away from the wall). McCabe et al. (2013) found $k_{\mathrm{wall}}$ = 1.0 gave good overtopping volumes for a particular recurve wall, and this value was used for this study.

The SWAB model solves these equations using a 1-dimensional semi-implicit finite-volume method. Input waves are applied within the model domain, using a method similar to that of Larsen and Dancy (1983). Reflected waves are absorbed by a sponge layer, using the method of Yoon and Choi (2000). Further details on the SWAB solver are provided by McCabe et al (2013).

The model has various options for incident wave type including the generation of random waves with a JONSWAP spectrum (McCabe, 2011). This ensures at least one wavelength is provided for the offshore sponge layer, and waves are non-breaking at the wave input location. The wave depth to wavelength ratio at the input location is in the range of 600m offshore, which is acceptable for the model equations. An onshore collection tank for overtopping water is also provided, so that it was assumed that water does not drain back into the sea. To some extent this is realistic of actual conditions given the flatness of Hulhumalé.

The model provides overtopping volumes as a time series of overtopping volumes: the cumulative volume of water passing over the seawall. This is based on the flow passing over the wall. Figure A1.3 illustrates an overtopping run using SWAB.

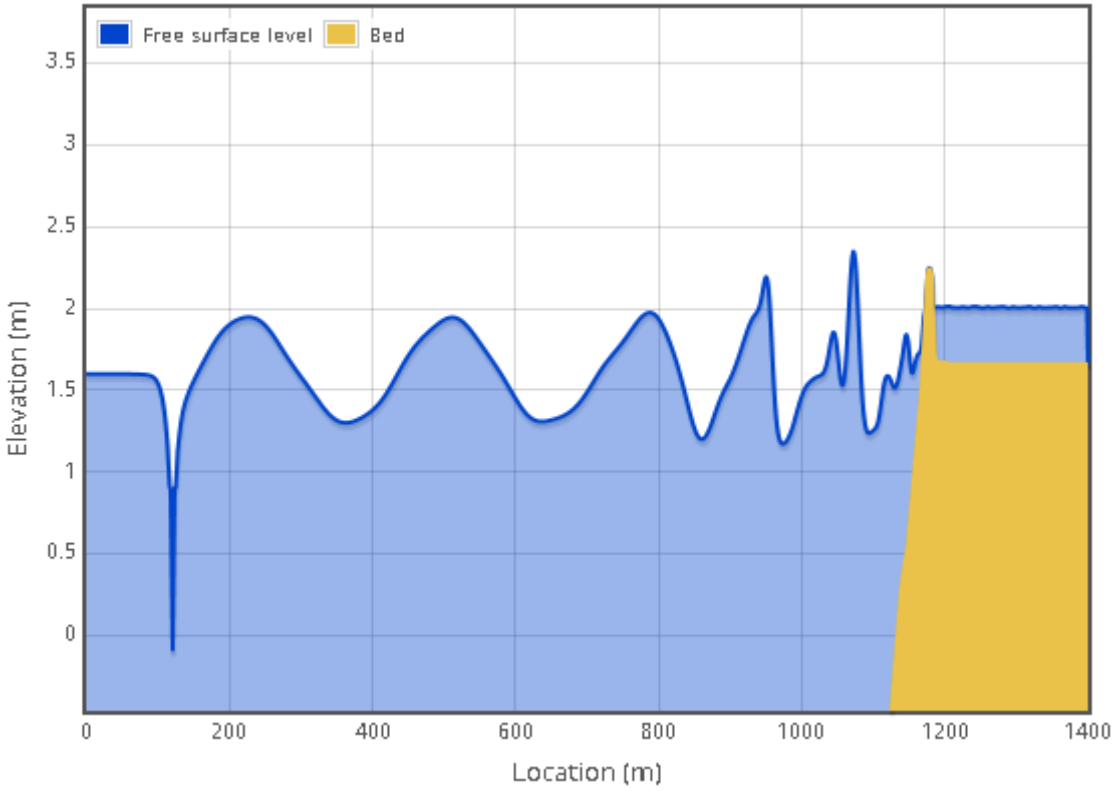


Figure A1.3 An example of wave generation and overtopping during a typically SWAB run.

## A2 Flood spread model

To translate the 1-dimensional SWAB outputs (which were used to generate an overtopping volume time series) to 2-dimenstional simulations of flooding, an inundation model, LISFLOOD-FP (Bates et al., 2010), was used. LISFLOOD-FP utilises raster 'storage cells' where each grid cell represents the local topography. For each flood simulation, this was represented by the overtopping volume per cell representing an input into each storage cell at the seaward boundary of the model's digital elevation model (DEM) (known as 'inflow points' which are located along the eastern defences on Hulhumalé). When storage cells are full, they flow into adjacent storage cells (Figure A2a). In the Hulhumalé DEM, flood cells are located 10m apart (Figure A2b). The flow depth ($h_{flow}$) represents the depth through which water can flow between two cells, and is defined as the difference between the highest water free surface in the two cells and the highest bed elevation.

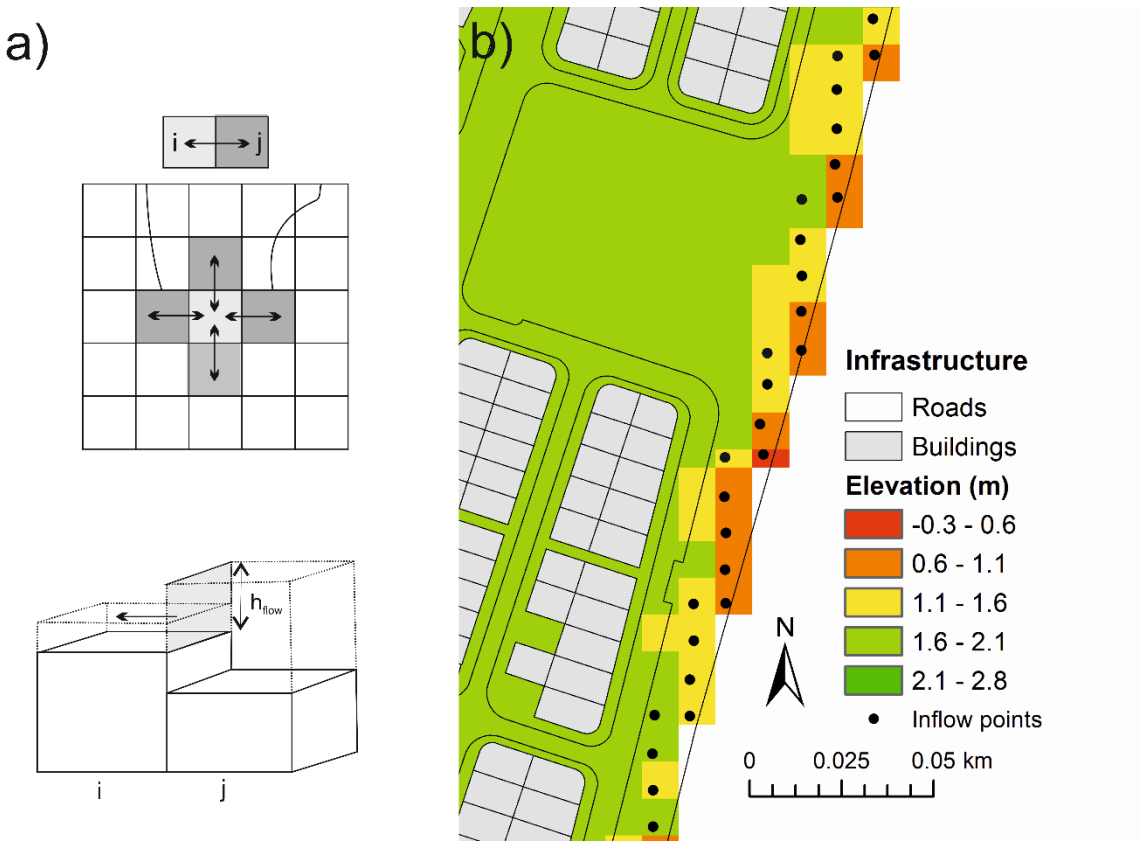


Figure A2. Representation of flow due to overtopping using LISFLOOD-FP. a) Flow between raster cells where the flow depth ($h_{flow}$) represents the depth through which water can flow between two cells (i, j) and is defined as the difference between the highest water free surface in the two cells and the highest bed elevation (adapted from Bates et al. 2005). b) Example of boundary inflow points on Hulhumalé.

When a cell is flooded, water is spread to the adjacent cells by solving a continuity and momentum equation (Equation A2.1) in two directions:

$$q_{t+\Delta t} = \frac{q_t - \mathrm{g}h_t \Delta t \frac{\partial (h_t + z)}{\partial x}}{\left(1 + \mathrm{g}h_t \Delta t \mathrm{n}^2 q_t / {h_t}^{10/3}\right)}$$

Equation A2.1

Where:

$g$ = gravity (m/s);
$h_t$ = water depth at time, t (m);
$n$ = Manning's friction coefficient;
$q_t$ = flow per unit width at time, t ($m^3 s^{-1}$);
$t$ = time (s);
$x$ = location in profile or grid domain (m);
$z$ = bed elevation (m).
$\Delta t$ = model time step (s);

Water depths were updated at each time step. As explained by Bates et al. (2013), there is an adaptive time step option in LISFLOOD-FP to aid stability, which is related to cell size and water depth, as specified in Equation A2.2. Resultantly the time step used by the solver varies throughout simulations (in the Hulhumalé case study, the time step was predominantly around 1s, and reducing to near 0.5s for the higher overtopping simulations). The stability criterion is given by the Courant–Freidrichs–Levy condition for shallow water flows such that the stable model time step, $\Delta$t, is a function of the grid resolution and the maximum water depth within the domain:

$$\Delta t_{\max} = \alpha \frac{\Delta x}{\sqrt{\mathrm{g}h_t}}$$

Equation A2.2

Where:
$g$ = gravity ($m\ s^{-1}$);
$h_t$ = the maximum water depth (m);
$\alpha$ = a dimensionless coefficient varies between 0.2 and 0.7 used to produce a stable simulation;
$\Delta t$ = model time step (s);
$\Delta x$ = model grid resolution in the direction x (m).

Water level time series at inflow locations were based upon the sea level time-series of a storm in May 2007 (the total sea water level was mainly affected by tide, with a surge influence, although surges are small in the Maldives as demonstrated in Wadey et al, 2017). However, as the Maldives are not low lying enough to be flooded by extreme still water levels alone (i.e. wave run-up is needed to project sea water onto land) (Wadey et al, 2017); the nation, like many other low-lying islands and coastal areas, is well-known to be susceptible to inundation from energetic swell (long-wavelength wind waves). Swell can propagate thousands of kilometres across ocean basins (Munk et al. 1963; Harangozo 1992; Hoeke et al. 2013; Wadey et al, 2017). Therefore this sea level time series was also associated with wave overtopping as the basis of a design storm (from conditions in May 2007). It assumed to have a linear relationship with the peak overtopping volume generated from SWAB. This was the only event where records or hindcasts exist where sea level and wave conditions are able to be quantified in relation to a significant flood . Hence, the results from this analysis were checked against local conditions reported at the time. Many of these reported local conditions are described in Wadey et al. (2017).

Outputs from LISFLOOD-FP indicated the area of land flooded and the average depth of flooding. The digital elevation model did not take account of buildings on the island.

### A3 Infrastructure affected

Outputs from LISFLOOD-FP were used to assess the infrastructure flooded using a Geographical Information System. The area flooded was overlaid on the infrastructure layer indicating whether or not the 1,295 buildings present on Hulhumalé at the time the research was undertaken were flooded (see Figure 1d in the main text). As rapid development is occurring, the number of buildings exposed and therefore potentially affected would have now increased.

## A4 Data for figures

Table A4.1 provides data for Figure 4. Data for other figures is not available due to data sensitivity and/or commercial issues.

Table A4.1 Data used to produce Fig 4 indicating the flood extent on Hulhumalé with sea-level rise and different adaptation strategies.

| | Do nothing | | | Build 0.5m sea wall | | | Build 1.0m sea wall | | | Build 1.5m sea wall | | | Build 0.5m sea wall plus nourish beach | | |
|---|---|---|---|---|---|---|---|---|---|---|---|---|---|---|---|
| SLR (m) | Volume (l/s/m) | Area (km^2) | No. of bdgs | Volume (l/s/m) | Area (km^2) | No. of bdgs | Volume (l/s/m) | Area (km^2) | No. of bdgs | Volume (l/s/m) | Area (km^2) | No. of bdgs | Volume (l/s/m) | Area (km^2) | No. of bdgs |
| 0 | 0 | 0.0 | 0 | 0 | 0.0 | 0 | 0 | 0.0 | 0 | 0 | 0 | 0 | 0 | 0 | 0 |
| 0.1 | 0 | 0.0 | 0 | 0 | 0.0 | 0 | 0 | 0.0 | 0 | 0 | 0 | 0 | 0 | 0 | 0 |
| 0.2 | 0 | 0.0 | 0 | 0 | 0.0 | 0 | 0 | 0.0 | 0 | 0 | 0 | 0 | 0 | 0 | 0 |
| 0.3 | 0 | 0.0 | 0 | 0 | 0.0 | 0 | 0 | 0.0 | 0 | 0 | 0 | 0 | 0 | 0 | 0 |
| 0.4 | 0 | 0.0 | 0 | 0 | 0.0 | 0 | 0 | 0.0 | 0 | 0 | 0 | 0 | 0 | 0 | 0 |
| 0.5 | 0 | 0.0 | 51 | 0 | 0.0 | 0 | 0 | 0.0 | 0 | 0 | 0 | 0 | 0 | 0 | 0 |
| 0.6 | 1.8 | 0.0 | 459 | 0.0 | 0.0 | 0 | 0 | 0.0 | 0 | 0 | 0 | 0 | 0 | 0 | 0 |
| 0.7 | 4.2 | 0.2 | 1202 | 0.5 | 0.0 | 459 | 0 | 0.0 | 0 | 0 | 0 | 0 | 0 | 0 | 0 |
| 0.8 | 14.6 | 0.2 | 1225 | 2.0 | 0.0 | 477 | 0 | 0.0 | 0 | 0 | 0 | 0 | 0 | 0 | 0 |
| 0.9 | 31.0 | 0.5 | 1281 | 8.4 | 0.0 | 602 | 1 | 0.0 | 66 | 0 | 0 | 0 | 0.1 | 0 | 0 |
| 1 | 54.2 | 0.8 | 1295 | 22.0 | 0.1 | 741 | 2 | 0.0 | 135 | 0 | 0 | 0 | 0.5 | 0 | 28 |
| 1.1 | 75.0 | 0.8 | 1295 | 31.3 | 0.2 | 753 | 7 | 0.0 | 405 | 1.0 | 0.0 | 64 | 2.0 | 0 | 113 |
| 1.2 | 95.0 | 1.1 | 1295 | 55.0 | 0.4 | 906 | 20 | 0.1 | 558 | 3.0 | 0.1 | 137 | 15.0 | 0.3 | 508 |
| 1.3 | 110.0 | 1.1 | 1295 | 64.4 | 0.7 | 912 | 43 | 0.2 | 732 | 11.0 | 0.2 | 434 | 41.0 | 0.7 | 711 |
| 1.4 | 135.0 | 1.2 | 1295 | 85.0 | 0.9 | 953 | 64 | 0.3 | 807 | 20.5 | 0.3 | 502 | 62.0 | 0.9 | 793 |
| 1.5 | 155.0 | 1.3 | 1295 | 105.0 | 1.0 | 999 | 85 | 0.6 | 877 | 48.0 | 0.6 | 651 | 83.0 | 1.0 | 865 |
| 1.6 | 200.0 | 1.4 | 1295 | 145.0 | 1.1 | 1044 | 112 | 0.7 | 888 | 70.0 | 0.7 | 689 | 111.0 | 1.0 | 883 |
| 1.7 | 200.0 | 1.7 | 1295 | 180.0 | 1.2 | 1210 | 130 | 0.9 | 973 | 100.0 | 0.9 | 831 | 136.0 | 1.3 | 1001 |
| 1.8 | 200.0 | 1.9 | 1295 | 200.0 | 1.9 | 1296 | 200 | 1.2 | 1296 | 130.0 | 1.2 | 973 | 200.0 | 1.9 | 1296 |

## A5 References


Bates, P.D., Dawson, R.J., Hall, J.W., Horritt, M.S., Nicholls, R.J., Wicks, J. & Hassan, M.A.A.M. (2005). Simplified two-dimensional numerical modelling of coastal flooding and example applications. *Coast. Eng*, 52 (9), 793-810. https://doi.org/10.1016/j.coastaleng.2005.06.001

Bates, P.D., Horritt, M.S. & Fewtrell, T.J. (2010). A simple inertial formulation of the shallow water equations for efficient two-dimensional flood inundation modelling. *J. Hydrol.*, 387, 33-45. https://doi.org/10.1016/j.jhydrol.2010.03.027

Bates, P., Trigg, M., Neal, J., Dabrowa, A. (2013). LISFLOOD-FP. Code release 5.9.6 [online]. https://www.bristol.ac.uk/media-library/sites/geography/migrated/documents/lisflood-manual-v5.9.6.pdf [accessed August 2016]

Harangozo, S.A., 1992. Flooding in the Maldives and its implications for the global sea level rise debate. In Woodworth, P.L., Pugh, D.T., DeRonde, J.G., Warrick, R.G. & Hannah, J. (eds), *Sea level changes: Determination and effects.* Geophysical monograph, volume 69. American Geophysical Union, pp. 95–99.

Hoeke, R.K., McInnes, K.L., Kruger, J.C., McNaught, R.J., Hunter, J.R. & Smithers, S.G. (2013). Widespread inundation of Pacific islands triggered by distant-source wind-waves. *Glob. Planet. Change,* 108, 128–138. https://doi.org/10.1016/j.gloplacha.2013.06.006

Kennedy, A.B., Chen, Q., Kirby, J.T. & Dalrymple, R.A. (2000). Boussinesq modeling of wave transformation, breaking and runup. I: 1D. *J Waterw Port C-ASCE*, 126 (1), 39–47. https://doi.org/10.1061/(ASCE)0733-950X(2000)126:1(39)

Larsen, J. & Dancy, H. (1983). Open boundaries in short wave simulations - a new approach. Coast. Eng., 7, 285–297. https://doi.org/10.1016/0378-3839(83)90022-4

Madsen, P.A. & Sorensen, O.R. (1992). A new form of the Boussinesq equations with improved linear dispersion characteristics. Part 2. A slowly varying bathymetry. Coast. Eng., 18, 183–204. https://doi.org/10.1016/0378-3839(91)90017-B

McCabe, M. (2011). Modelling nearshore waves, runup and overtopping. PhD thesis, University of Manchester, UK.

McCabe, M.V., Stansby, P.K. & Apsley, D.D. (2013). Random wave runup and overtopping a steep sea wall: Shallow-water and Boussinesq modelling with generalised breaking and wall impact algorithms validated against laboratory and field measurements. Coast. Eng., 74, 33-49. https://doi.org/ 10.1016/j.coastaleng.2012.11.010

Munk, W.H., Miller, G., Snodgrass, F. & Barber, N. (1963). Directional recording of swell from distant storms. Philos. Trans. R. Soc. Lond. A. 255, 505–584. https://doi.org/10.1098/rsta.1963.0011

Stansby, P., Chini, N., Apsley, D., Borthwick, A., Bricheno, L., Horrillo-Caraballo, J., McCabe, M., Reeve, D., Rogers, B.D., Saulter, A., Scott, A., Wilson, C., Wolf, J. & Yan, K. (2013). An integrated model system for coastal flood prediction with a case history for Walcott, UK, on 9th November 2007. *J. Flood Risk Manag*., 6(3), 229-252. https://doi.org/ 10.1111/jfr3.12001.

Wadey, M., Brown, S., Nicholls, R.J. & Haigh, I. (2017). Coastal flooding in the Maldives: An assessment of historic events and their implications. *Nat. Hazards.* 89, (1), 131-159.. https://doi.org/10.1007/s11069-017-2957-5

Yoon, S.B. & Choi, J.W. (2001). A note on extension of fully dispersive weakly nonlinear wave equations for rapidly varying topography. *Coast. Eng. J*., 43 (3),143–160. https://doi.org/10.1142/S0578563401000323